Violation of the orbital depairing limit in a nonunitary state: High-field phase in the heavy fermion superconductor UTe_2

Kazushige Machida
Department of Physics, Ritsumeikan University, Kusatsu 525-8577, Japan

(Received 12 January 2023; revised 24 April 2023; accepted 9 June 2023; published 21 June 2023)

A theoretical study is reported on the origin of an extremely high upper critical field ∼70 T observed in UTe_2 with the transition temperature $T_c = 1.6$–2 K, which exceeds the conventional orbital depairing limit set by the Fermi velocity and T_c for a superconductor (SC) in the clean limit. We investigate possible violation of the orbital limit in terms of a spin-triplet nonunitary state, which is effectively coupled to the underlying magnetization induced by an external field. This produces the reduced internal field by canceling it via magnetization. We formulate a theory within the Ginzburg-Landau framework to describe this orbital limit violation and analyze experimental data on the upper critical fields for various field orientations in UTe_2. We show that the orbital limit violation for a spin-triplet SC, as well as the Pauli-Clogston limit violation for a spin-singlet SC, constitutes a complete and useful framework for examining the high field physics of superconductors in the clean limit.

DOI: 10.1103/PhysRevB.107.224512

I. INTRODUCTION

A recently found heavy Fermion superconductor (SC) UTe_2 has attracted much interest because it is a candidate material of a triplet pairing, which is rare except for superfluid ^{3}He [1,2] and UPt_3 [3–6]. They are all characterized by multiple phases owing to rich internal degrees of freedom inherent to a spin-triplet pairing. UTe_2 is known to exhibit remarkable superconducting properties in addition to multiple phases in magnetic field (H) and temperature (T) planes under both ambient and applied pressure [7]. In the superconducting energy gap structure probed by several thermodynamic measurements [7–9], a pair of point nodes is located along the a axis in orthorhombic crystals. The time reversal symmetry is broken in the superconducting phase detected by the Kerr rotation experiment [10]. A scanning tunneling microscopy (STM) experiment suggested that the chiral superconductivity may be achieved [11].

According to a series of ^{125}Te NMR experiments [12–16], the Knight shift (KS) or spin susceptibility drops (remains uncharged) along the b and c axes (the a axis) below the superconducting transition temperature T_c at low fields, indicating that the d-vector points perpendicular to the a axis. In other words, the d-vector has the components along the b and c axes. At the lowest fields along the b axis, the KS decreases, but as H increases from 5 T up to ∼12 T the KS as a function of H gradually ceases decreasing to return to the normal value. This implies that the d-vector changes its direction to be perpendicular to the applied field direction parallel to the b axis to gain the Zeeman energy. Along the c axis, the KS as a function of H begins increasing from the lowest field and continuously returns to the normal value at approximately 5 T. Thus the d-vector should be the three components along all the three directions with complex numbers. In other words, the superconducting order parameters must have three dimensional vectorial structures with three components. This d-vector rotation phenomenon plays a crucial role in understanding the field reinforced high field phase.

In this paper, we focus on the following experiments [7].

(1) The upper critical field H_{c2} is extremely high, reaching ∼70 T compared with $T_c = 1.6$–2.0 K.

(2) The H-T phase diagram along the magnetic hard b axis consists of two phases: low field (LSC) and high field phases (HSC). In the HSC, $H_{c2}(T)$ has an unusual positive slope, i.e., $dH_{c2}(T)/dT > 0$.

(3) When tilting H toward the magnetic easy a axis from the b axis by small angles φ up to only $\varphi \sim 7^\circ$, the HSC quickly diminishes from the H-T phase diagram, leaving the LSC whose $H_{c2} \sim 10$ T.

(4) When the field direction changes from the b axis toward the other magnetic hard c axis by the angle θ measured from the b axis, the HSC also diminishes up to a slightly larger angle $\theta \sim 12^\circ$, beyond which only the LSC remains. However, at $\theta \sim 35^\circ$ the isolated HSC detached from the LSC appears above the so-called meta-magnetic transition field H_m at which the b axis magnetization curve $M_b(H)$ exhibits a jump via a first-order phase transition.

As neither quantitative nor qualitative explanation exists for these remarkable facts of UTe_2, we attempt to understand some of these phenomena theoretically qualitatively. In particular, we address the following problems.

(A) What determines the upper limit of H_{c2}? In a clean limit superconductor [17], which we assume here, the orbital limit of H_{c2} without the Pauli paramagnetic effect is given by $H_{c2}^{orb} = \Phi_0/2\pi\xi^2$, where Φ_0 is the flux quantum, and the coherent length $\xi = \hbar v_F/\pi T_c$. The Fermi velocity v_F measured recently by the dHvA experiment [18] is $v_F^\alpha \sim 11.0$ km/s and $v_F^\beta \sim 6.3$ km/s, yielding $H_{c2}^{orb} \sim 12$ T. This closely matches $H_{c2} \sim 10$ T for the LSC, but is significantly less than the observed maximal $H_{c2}(\theta = 35^\circ) \sim 70$ T. Note that according to the H_{c2} analysis by Rosuel *et al.* [19] and Helm *et al.* [20],

the estimated v_F required to explain $H_{c2} \sim 70$ T is 6.7–7.1 km/s albeit $T_c \sim 3$ K, meaning that the high and low field phases are governed by the same Fermi surface structure. Thus we must understand the mechanism that causes the violation of the orbital depairing limit.

(B) Why does $H_{c2} \parallel$ b in the HSC have a positive slope and terminates abruptly only at $H_m = 34$ T and reappears above H_m at approximately $\theta = 35^\circ$ between the b and c axes [19–21]? Why is it not between the b and a axes?

In this paper, to address these issues, we assume a spin-triplet pairing with a nonunitary form [22] characterized by a complex d-vector with three components. This nonunitary state quite successfully describes not only UTe_2 but also other SCs such as URhGe and UCoGe. These are all magnetization-tuned superconductors [23–25].

The main advance from our previous series of papers [23–25] lies on the point that we can clarify the origin of the concept of the absolute upper limit of H_{c2}, namely H_{c2}^{AUL}, which was introduced in an ad hoc manner in Refs. [23–25]. That is, as these papers describe in detail, because $dH_{c2}/dT > 0$ in some region of the H-T phase diagrams, H_{c2} becomes unbound. We had to introduce H_{c2}^{AUL} to avoid this unphysical scenario "by hand." Now, in this paper, we clarify the origin of H_{c2}^{AUL}, leaving intact the main body of our arguments based on a spin triplet nonunitary state. Simultaneously, this enables us to establish a general concept for the violation of the orbital depairing limit in a nonunitary state. Thus the present theory is applicable not only to UTe_2 but also to more general superconductors, providing a mechanism for attaining high field superconductors by exceeding both the orbital depairing and Pauli depairing limits. This novel mechanism of the enhancement and limitation of H_{c2} associated with H_{c2}^{AUL} may explain the reason a certain class of superconductors in which globally or locally centrosymmetry is broken exhibit abnormally high H_{c2}.

This paper is arranged as follows. First, we briefly describe our nonunitary triplet theory developed previously [23–25] in Sec. II. To understand a mechanism of the violation of the orbital depairing limit of H_{c2} we employ a simple Ginzburg-Landau (GL) formalism to illustrate our basic concept as clearly as possible in Sec. III. The proposed mechanism is applied to UTe_2. We analyze various experimental data on H-T phase diagrams for various field orientations in Sec. IV. In Sec. V, we devote to discussions and perspectives to deepen our understanding on the physics associated with UTe_2 and other sister compounds, URhGe and UCoGe. The topics include the classification scheme of the pairing symmetry, the concept of the d-vector rotation, possible chiral-nonchiral transition in high fields. Section VI presents the summary and conclusion.

II. THEORETICAL FRAMEWORK

A. Preliminaries to Ginzburg-Landau theory

To answer the above questions (A) and (B), we begin with the most generic GL theory for a spin triplet state. Here, we summarize our previous theory for further developments [23–25].

We assume a nonunitaty A-phase-like pairing state described by the complex **d**-vector

$$\mathbf{d}(k) = \phi(k)\boldsymbol{\eta} = \phi(k)(\boldsymbol{\eta}' + i\boldsymbol{\eta}'') \quad (1)$$

($\boldsymbol{\eta}'$ and $\boldsymbol{\eta}''$ are real vectors) among the odd-parity pairing states. $\phi(k)$ is the orbital part of the pairing function which is not specified in the main part of this paper because its form is irrelevant for the present arguments. The pairing function is classified under the overall symmetry

$$\mathrm{SO}(3)^{\mathrm{spin}} \times D_{2h}^{\mathrm{orbital}} \times U(1)^{\mathrm{guage}} \quad (2)$$

with the spin, orbital, and gauge symmetry, respectively [26,27]. We assume the weak spin-orbit coupling scheme [28,29]. This assumption is justified by the d-vector rotation beginning from the low fields, $\sim$1 T for the c axis [14], and $\sim$5 T for the b axis [13], indicating that the spin-orbit coupling is weak that locks the d-vector to crystalline lattices.

We note that the $\mathrm{SO}(3)^{\mathrm{spin}}$ symmetry is applied to the Cooper pairs in the many-body sense and the normal state electrons are under the strong spin-orbit coupling in the one-body sense. The latter leads to the anisotropic magnetic behaviors. Note that we are treating a composite electron system, consisting of the itinerant electron system with a heavy mass responsible for the SC formation and the localized electron system at the U atomic sites for the underlying magnetic behaviors. Both subsystems result primarily from the same $5f$ electrons on the U atoms. This dichotomy, associated with strongly renormalized $5f$ electron with the enhanced mass, is not considered here as it is beyond the scope of the present paper. Thus the $\mathrm{SO}(3)^{\mathrm{spin}}$ symmetry is perturbed by the latter localized moments through the effective spin-orbit coupling whose strength is difficult to evaluate microscopically. Here, we consider it phenomenologically, as described shortly. This $\mathrm{SO}(3)^{\mathrm{spin}}$ triple spin symmetry is expressed in terms of a complex three component vectorial order parameter $\boldsymbol{\eta} = (\eta_a, \eta_b, \eta_c)$.

As mentioned earlier, the spin rotation symmetry is weakly broken through the spin-orbit coupling (SOC) whose magnitude depends the crystalline direction and determines the strength of the d-vector rotation field. In contrast, in the limit of the strong SOC, the d-vector never rotates under a finite magnetic field because the spin symmetry is reduced to the crystalline symmetry D_{2h}, yielding four one-dimensional irreducible representations. Thus our framework based on the weak SOC is sufficiently flexible to include the strong SOC as a limit. As detailed in the following, the three components of the order parameter originally the same transition temperatures under the spin rotational symmetry, which is broken by either applied field and the influence of the underlying magnetic subsystem.

Under $\mathrm{D}_{2h}^{\mathrm{orbital}}$ symmetry, the most general GL free energy functional up to the quadratic order is expressed by

$$F^{(2)} = a_0(T - T_{c0})\boldsymbol{\eta}\cdot\boldsymbol{\eta}^* + b|\mathbf{M}\cdot\boldsymbol{\eta}|^2 + i\kappa\mathbf{M}\cdot\boldsymbol{\eta}\times\boldsymbol{\eta}^*, \quad (3)$$

where b is a positive constant. The last invariant above results from the nonunitarity of the pairing function in the presence of the spontaneous moment $\mathbf{M}(H)$, which breaks the $\mathrm{SO}(3)^{\mathrm{spin}}$ spin symmetry. Without loss of generality, we assume $\kappa > 0$, but we warn that it can be negative in UTe_2. This term responds to external field directions differently.

It is convenient to introduce

$$\eta_{\pm} = \frac{1}{\sqrt{2}}(\eta_b \pm i\eta_c) \tag{4}$$

for $\mathbf{M} = (M_a, 0, 0)$, where we define the a axis as the magnetic easy axis. η_+ (η_-) corresponds to the spin up-up (down-down) pair or the $A_1(A_2)$ phase. Note that the spin quantization axis is defined relative to the $\mathbf{M}$ direction, i.e., the magnetic easy a-axis here. Because of the magnetic coupling term $i\kappa\mathbf{M}\cdot\boldsymbol{\eta}\times\boldsymbol{\eta}^*$, the spin direction for the Cooper pair may change.

From Eq. (3), the quadratic term $F^{(2)}$ becomes

$$F^{(2)} = a_0\{(T-T_{c1})|\eta_+|^2 + (T-T_{c2})|\eta_-|^2 + (T-T_{c3})|\eta_a|^2\} \tag{5}$$

with

$$T_{c1,2}(M_a) = T_{c0} \pm \frac{\kappa}{a_0}M_a,$$
$$T_{c3}(M_a) = T_{c0} - \frac{b}{a_0}M_a^2. \tag{6}$$

Note that the actual second transition temperature is modified to $T'_{c2} = T_{c0} - (\kappa M_a/a_0)(\beta_1-\beta_2)/2\beta_2$ because of the fourth order GL terms [23–25], but we ignore this correction and maintain the expression of Eq. (6) for clarity of our arguments.

The root-mean-square average $\sqrt{\langle M_a^2\rangle}$ of the FM fluctuations along the magnetic easy a axis is simply denoted by M_a and acts to shift the original transition temperature T_{c0} and split it into T_{c1}, T_{c2}, and T_{c3} expressed by Eq. (6). According to this, T_{c1} (T_{c2}) increases (decreases) linearly as a function of M_a, whereas T_{c3} decreases quadratically as M_a^2 from the degeneracy point $M_a = 0$. The three transition lines meet at $M_a = 0$, where the three components η_i ($i = +, -, a$) are all degenerate. Thus, away from the degenerate point at $M_a = 0$, the A_0 phase beginning at T_{c3} quickly disappears from the phase diagram. Below T_{c2} (T_{c3}), the two components η_+ and η_- coexist, symbolically denoted by $A_1 + A_2$. Note that, because their transition temperatures are different, $A_1 + A_2$ is not the so-called A-phase, which is unitary, but is generically nonunitary except at the degenerate point $M_a = 0$ where the totally symmetric phase is achieved with the time reversal symmetry preserved. Thus the $A_1 + A_2$ phase is the so-called distorted A phase [1]. Similarly, below T_{c3}, all the components coexist; $A_1 + A_2 + A_0$ is realized. We explain it more in detail in the Appendix. The naming such as A_1, A_2, and A_0 is retained even when the spin quantization axis change according to the d-vector rotation under fields.

The magnetic coupling κ, which is a key parameter for characterizing UTe_2, is originally estimated [30] as $\kappa = T_c\frac{N'(0)}{N(0)}ln(1.14\omega/T_c)$, where $N'(0)$ is the energy derivative of the normal DOS, and ω is the energy cutoff. This term results from the electron-hole asymmetry near the Fermi level. κ indicates the degree of this asymmetry. This may be significant for a narrow band or the Kondo coherent band in the heavy Fermion material UTe_2. We can estimate $N'(0)/N(0) \sim 1/E_F$ with the Fermi energy E_F. Because $T_c = 2$ mK and $E_F = 1$ K in ^{3}He, $\kappa \sim 10^{-3}$, while for UTe_2 $T_c \sim 1$ K and $E_F \sim T_K$ with the Kondo temperature $T_K \sim 30$ K [7]. $\kappa \sim 10^{-1}$. We also note that the sign of κ can be either positive or negative, depending on the detailed energy dependence at the Fermi level because it is $\propto N'(0)$. If $\kappa > 0$ ($\kappa < 0$), the up-up (down-down) pair appears at higher T. Thus the KS remains unchanged (decreases) below T_{c1}.

In the following discussions, we consider a case in which the two components η_+ and η_- are nonvanishing, ignoring the third component η_a because, under ambient pressure, UTe_2 exhibits the two phases LSC and HSC, corresponding to η_+ and η_-, respectively. The current UTe_2 samples with $T_c = 1.6$ K exhibit a single transition under $H = 0$ because $T_{c2} < 0$, as evidenced by the significant residual density of states. The second transition is only realized at a finite field for $H \parallel b$ axis. However, we expect that the second transition $T_{c2} > 0$ might be realized for samples with $T_c = 2$ K without the residual density of states. Note that, under pressure, the third component becomes relevant [24] (see also Appendix for the third transition). Hereinafter, we redefine the notation $\kappa/a_0 \to \kappa$.

III. UPPER CRITICAL FIELD

Under an applied field with the vector potential $\mathbf{A}$, the gradient GL energy is given under D_{2h}^{orbital} symmetry

$$F_{\text{grad}} = \sum_{\nu=a,b,c}\{K_a|D_x\eta_\nu|^2 + K_b|D_y\eta_\nu|^2 + K_c|D_z\eta_\nu|^2\}, \tag{7}$$

where K_a, K_b, and K_c are the effective masses along the a, b, and c axes, respectively. $D_i = -i\nabla_i + \frac{2\pi}{\Phi_0}A_i$ is the gauge invariant derivative, with Φ_0 being the quantum flux and A_i the vector potential component. This form of Eq. (7) shows that the H_{c2} for the three components each starting at T_{cj} ($j = 1, 2, 3$) intersect each other, never avoiding or leading to a level repulsion. The level repulsion may occur for the pairing states belonging to multidimensional representations (see, for example, Refs. [31–34] in UPt_3). The external field H also passes through $M_a(H)$ in addition to the vector potential $\mathbf{A}$, which results in the orbital depairing.

Thus each component is independent within the quadratic terms. The GL free energy density F under the external magnetic field H in terms of the superconducting order parameter $\eta_\pm$ is given by

$$F = \sum_{i=\pm}\{a_0(T-T_{c,i})|\eta_i|^2 + K_a|D_x\eta_i|^2 + K_b|D_y\eta_i|^2 + K_c|D_z\eta_i|^2\}. \tag{8}$$

The variation with respect of η_i^* leads to the GL equation

$$a_0(T-T_c)\eta_i + \left(K_aD_x^2 + K_bD_y^2 + K_cD_z^2\right)\eta_i = 0. \tag{9}$$

Following the standard procedure [35], the upper critical field H_{c2} is obtained as the lowest eigenvalue of the linearized GL equation or Schrödinger type equation of a harmonic oscillator, i.e.,

$$H_{c2,j}^{(+)}(T) = \alpha_0^j(T_{c0} + \kappa M_a - T),$$
$$H_{c2,j}^{(-)}(T) = \alpha_0^j(T_{c0} - \kappa M_a - T) \tag{10}$$

with $j = a$, b, and c axis. We introduce the coefficients

$$\alpha_0^a = \frac{\Phi_0}{2\pi\sqrt{K_b K_c}} a_0, \quad \alpha_0^b = \frac{\Phi_0}{2\pi\sqrt{K_c K_a}} a_0,$$
$$\alpha_0^c = \frac{\Phi_0}{2\pi\sqrt{K_a K_b}} a_0. \tag{11}$$

These coefficients determine the initial slopes of the upper critical fields. $H_{c2,j}^{(+)}$ and $H_{c2,j}^{(-)}$ are the upper critical fields for the spin up-up and down-down pairs, or the A_1 and A_2 phases, respectively.

Expressing Eq. (10) in a generic form

$$H_{c2} - \alpha_0 \kappa M(H_{c2}) = \alpha_0 (T_{c0} - T). \tag{12}$$

The right-hand side of Eq. (12) is simply

$$H_{c2}^{\rm orb}(T) = \alpha_0 (T_{c0} - T) \tag{13}$$

for an unperturbed upper critical field owing to the orbital depairing limit with T_{c0} whose maximum value is given by $H_{c2}^{\rm orb}(T = 0) = \alpha_0 T_{c0}$. On the left-hand side of Eq. (12), we define the effective field

$$H_{\rm eff} = H_{\rm ext} - \alpha_0 \kappa M(H_{\rm ext}). \tag{14}$$

This implies that the external field $H_{\rm ext}$ is reduced by the amount of $\alpha_0 \kappa M(H_{\rm ext})$. The upper bound of the orbital depairing field of $H_{c2}^{\rm orb}(T)$ for the a axis, for example, is determined by

$$H_{c2}^{\rm orb}(T \to 0) = \alpha_0^a T_{c0} = \frac{\Phi_0}{2\pi\sqrt{K_b K_c}} a_0 T_{c0}. \tag{15}$$

Consequently, this is given by the expression in the clean limit: $H_{c2}^{\rm orb}(T) = \Phi_0 / 2\pi\xi^2$, where the coherence length $\xi = \hbar v_{\rm F} / \pi T_{c0}$. Namely, at $H_{c2}^{\rm orb}(0)$ the inter-vortex distance becomes comparable to the core size ξ. This generally results in the absolute value of the upper limit of $H_{c2}^{\rm orb}(0)$. To break this absolute upper limit due to the orbital depairing, we must reduce the effective magnetic field $H_{\rm eff}$ from the external field $H_{\rm ext}$. This concept is the same as that developed for a spin singlet pairing [36] and similar to the so-called Jaccarino-Peter mechanism [37]. Henceforth, we surpress the subscript "ext"; thus, $H_{\rm ext} \to H$.

It is clear that at $T = 0$, the absolute value of $H_{\rm eff}$ is bounded by

$$|H_{c2} - \alpha_0 \kappa M(H_{c2})| \leqslant H_{c2}^{\rm orb}(T = 0) = \alpha_0 T_{c0} \tag{16}$$

for $H_{c2}(0)$ to be a solution. Thus $H_{c2}(0)$ can be enhanced at $T \to 0$.

Let us now examine the typical cases for several magnetization curves, as shown in Fig. 1. We first consider the simplest case where the magnetization curve is given by $M(H) = \chi H$, as depicted in the upper panel of Fig. 1(a). Because $H_{\rm eff}$ is reduced by the presence of $M(H)$ in Eq. (14) [the middle panel in Fig. 1(a)], we obtain

$$H_{c2}(T) = \frac{H_{c2}^{\rm orb}(T)}{1 - \alpha_0 \kappa \chi}, \tag{17}$$

where $1 - \alpha_0 \kappa \chi$ is the enhancement factor relative to $H_{c2}^{\rm orb}(T)$ [the bottom panel in Fig. 1(a)]. Thus, in principle, $H_{c2}(T)$ increases indefinitely toward the critical point $\alpha_0 \kappa \chi = 1$ from below. As a general tendency, when the magnetization becomes saturated at higher field, $H_{c2}(T)$ eventually tends to be finite.

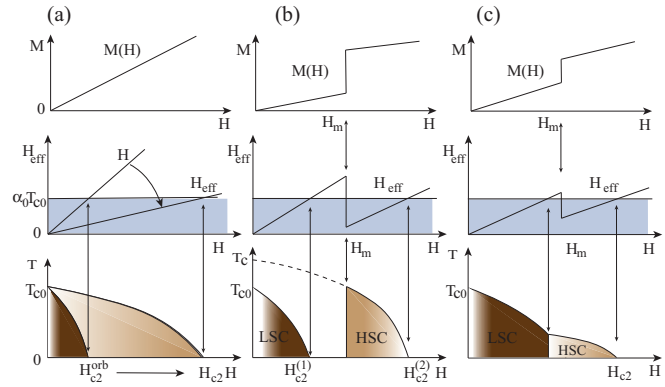

FIG. 1. (a) Case of a magnetization curve $M(H) = \chi H$ (top). $H_{\rm eff}$ is reduced compared with the external field. The permitted region with light blue color bounded by $\alpha_0 T_{c0}$ extends to a higher field (middle). H_{c2} is enhanced compared with $H_{c2}^{\rm orb}$ (bottom). (b) When the magnetization has the jump at the metamagnetic field $H_{\rm m}$, $H_{\rm eff}$ goes outside the allowed region at $H_{c2}^{(1)}$. However, it returns above $H_{\rm m}$ and HSC appears, separated from LSC. The extrapolated $T_{\rm c}$ for HSC is higher than T_{c0} for LSC (dotted curve in the bottom panel). (c) The metamagnetic jump is smaller than the case in (b). LSC and HSC overlap to appear. The light blue regions in the middle panels in (a), (b), and (c) show the permitted region for H_{c2}.

Next, we consider a case in which the magnetization curve jumps at the metamagnetic transition at $H_{\rm m}$, as shown in the upper panel of Fig. 1(b). $H_{\rm eff}$ exceeds the permitted maximum region set by $\alpha_0 T_{c0}$ in Eq. (14) at a lower field, as shown in the middle panel of Fig. 1(b). Thus the low SC (LSC) phase is terminated at $H_{c2}^{(1)}(T)$ (see the bottom panel of Fig. 1(b)). However, immediately above $H_{\rm m}$, $H_{\rm eff}$ reenters the allowed region, as indicated in light blue in the middle panel. Thus high SC (HSC) occurs from $H_{\rm m}$ to $H_{c2}^{(2)}(T)$, as shown in the bottom panel of Fig. 1(b). In this case, LSC and HSC are separated in H-T phase diagram shown in the bottom panel in Fig. 1(b).

Depending on the magnetization curve with the metamagnetic transition, a different scenario may occur as shown in Fig. 1(c). Because $H_{\rm eff}$ defined in Eq. (14) is determined by the combination of $M(H)$ and the coupling constant $\alpha_0 \kappa$, the two SC phases of LSC and HSC overlap, as shown in the bottom panel of Fig. 1(c). This is in contrast with the case mentioned above in which LSC and HSC are separated by the normal state along the H axis in H-T phase diagram. Note that in these examples, LSC and HSC are the same pairing state.

IV. ANALYSIS OF $H_{c2}(T)$ in UTe_2

A. $H//b$

In this section, we examine the H-T phase diagram in UTe_2 for $H \parallel b$ by applying the previous general considerations based on GL theory for nonunitary pairing. To explain various mysteries associated with the phase diagram for $H \parallel b$, we must know the magnetization curve $M(H)$ in $H \parallel b$. According to a measurement by Miyake *et al.* [38,39] $M(H)$ has the

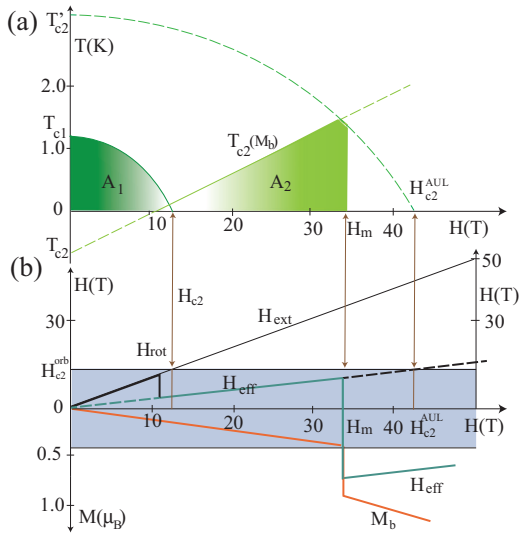

FIG. 2. (a) Resulting H-T phase diagram with the A_1 (LSC) and A_2 (HSC) phases. The dashed lines are not realized. (b) Constructed $H_{\rm eff}$ (green curve) at $T = 0$ as a function of the external field H using the measured magnetization curve [38] of $M_b(\mu_B)$ (red curve). $H_{\rm rot}$ is the d-vector rotation field. $H_{\rm m}$ is the metamagnetic transition field. $H_{c2}^{\rm AUL}$ is the absolute upper limit of H_{c2}.

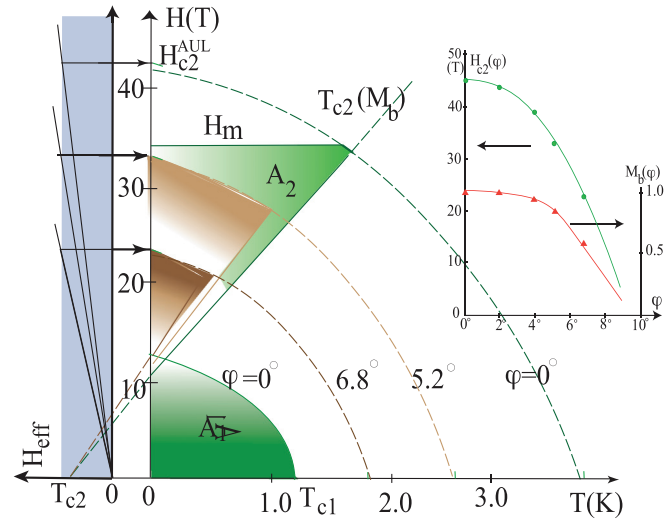

FIG. 3. Phase diagram in the H-T plane for $H \parallel b$ and the field orientations tilted by the angle φ measured from the b axis toward the a axis. A_2 or HSC quickly shrinks as φ increases, whereas A_1 or LSC remains almost unaffected. $H_{c2}^{\rm AUL}(\varphi)$ becomes low as φ increases indicated by the left-hand side because the projection of $M_b(\varphi)$ strongly decreases as postulated in the inset. The resulting upper critical field $H_{c2}(\varphi)$ is shown.

metamagnetic transition at $H_{\rm m} = 34T$ via a first order with the large magnetization jump, which is indicated by the red curve of M_b in Fig. 2(b). Accordingly, the effective field $H_{\rm eff}$ (green curve) exhibits a sharp drop at $H_{\rm m}$. By selecting an appropriate parameter value for $\alpha_0\kappa$, which is only the adjustable parameter in our theory, we can reproduce the experimental data. That is, $H_{\rm eff}$ is reduced below $H < H_{\rm m}$ as seen by the green curve of Fig. 2(b). However, beyond $H_{\rm m}$, it exceeds the limit of the permitted region denoted by the light blue band.

In Fig. 2(a), the A_1 phase starts at T_{c1} and disappears at a lower field because the Cooper pair polarization points to the a axis, as evidenced by the KS experiment [12–16]. In low fields, KS remains unchanged (drops) for the a-axis (b- and c-axis) field. Thus, for the A_1 phase $H_{\rm eff} = H$ because of $\mathbf{d} \times \mathbf{d}^* \perp M_b$.

In contrast, the A_2 phase with the increasing T_{c2} changes the d-vector direction during the d-vector rotation for the field range 5–12 T such that $\mathbf{d} \times \mathbf{d}^* \parallel M_b$. Thus $T_{c2} = T_{c0} + \kappa M_b(H)$ instead of M_a originally given in Eq. (6), or T_{c2} increases with $M_b(H)$ as shown in Fig. 2(a). However, even if T_{c2} is increasing indefinitely, the A_2 phase ceases to exist above $H_{\rm m}$ because $H_{\rm eff}$ exceeds the limit. It terminates at $H_{c2}^{\rm AUL}$, where, as indicated by the dotted line of Fig. 2(b) the extrapolated $H_{\rm eff}$ from below exceeds the limit. This defines the absolute upper limit of H_{c2}, or $H_{c2}^{\rm AUL}$, which is given by $H_{c2}^{\rm AUL} = \alpha_0(T'_{c2} - T)$, where T'_{c2} is not realized. Note that a part of $H_{c2}^{\rm AUL}(T)$ is realized where $H_{\rm eff}$ is still within the permitted region [Fig. 2(a)]. These constitute the whole A_2 phase shown in Fig. 2(a).

B. b to a

When the magnetic field is tilted from the magnetic hard b axis toward the magnetic easy a axis by the angle φ measured from b, the HSC phase quickly diminishes from the H-T phase diagram up to $\varphi \sim 7°$, whereas LSC remains the same. To understand this intriguing behaviors, we apply the same concept described above by postulating $M_b(\varphi)$ as a function of φ. When tilting the field direction away from the b axis, $M_b(\varphi)$ generally decreases because the M_b component projecting onto the field direction becomes small. Therefore $H_{\rm eff}(\varphi)$ increases with φ, as shown in the left-hand side of Fig. 3, implying that $H_{c2}^{\rm AUL}(\varphi)$ is lowered. The resulting $H_{c2}^{\rm AUL}(\varphi)$ is plotted by the dotted curves in Fig. 3 for the selected angles. Because $T_{c2}(\varphi) = T_{c0} + \kappa M_b(\varphi)$ becomes sharper to rise or $T_{c2}(\varphi)$ at T_{c2} rotates counterclockwise as depicted in Fig. 3, the A_2 regions with the triangle areas (brown color) shrink and disappear from the H-T phase diagram.

The postulated $M_b(\varphi)$ behavior to reproduce the phase diagram is depicted in the inset of Fig. 3, which exceeds that expected by simple projection of $M_b(\varphi)$ onto the field direction. $M_b(\varphi)$ decreases quickly upon tilting by a few degrees, which is noteworthy. This might be understandable because the magnetic easy a axis is special; The moment M_b tends to redirect toward the easy a axis to gain the magnetic energy by increasing the M_a component. Thus the rotation of the moment direction of M_b may be larger than the simple projection count. A similar large change of the magnetization curve by small tiltings of the field direction is observed in URhGe from the hard to easy axis case [40]. Reflecting the strong decrease in $M_b(\varphi)$, the resulting $H_{c2}(\varphi)$ sharply drops as depicted in the inset of Fig. 3.

C. b to c

We examine the phase diagram for the field orientation tilted from the b axis to the other hard axis c axis by the angle θ measured from the b axis to understand the isolated HSC

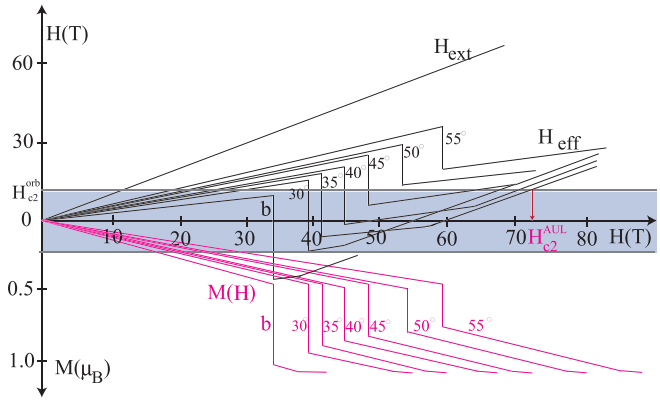

FIG. 4. Magnetization curve $M_b(H)$ (red curve) for $H \parallel b$ axis obtained experimentaly [38,39]. The other magnetization curves for various angles of θ are reconstructed by projecting $M_b(H)$ onto the magnetic field direction. $H_{\rm eff}(\theta) = H - \alpha_0\kappa M(\theta)$ is constructed from $M(\theta)$ thus obtained. The light blue band at the center indicates the permitted region for H_{c2}. The intersection point between $H_{\rm eff}(\theta)$ and the light blue band yields the absolute upper limit $H_{c2}^{\rm AUL}$.

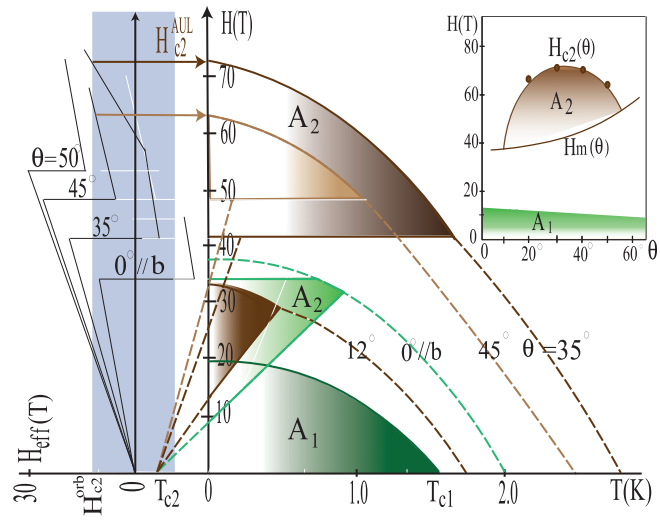

FIG. 5. H-T phase diagram for various θ, including the case $H \parallel b$ axis for comparison. The permitted region of $H_{\rm eff}$ is indicated on the left-hand side in light blue, which is the same as in Fig. 4. For $\theta = 35^\circ$, HSC (A_2) is permitted for $H_{\rm m} < H_{\rm eff} < H_{c2}^{\rm AUL}$. The H_{c2} curve starts at $H_{c2}^{\rm AUL}$ toward T_{c2} at $H = 0$. However, the HSC terminates abruptly at $H_{\rm m}$, below which $H_{\rm eff}$ is outside the permitted region. The permitted region at the low field is not available for the A_2 because $T_{c2} < 0$. It is used by LSC (A_1), which is relatively unchanged with varying θ, including the case for $H \parallel b$ axis. The inset shows the HSC (A_2) and LSC (A_1) as a function of θ.

phase whose maximum H_{c2} reaches ~70 T, which exceeds the orbital depairing upper critical field.

Let us begin to evaluate the magnetization curves $M_b(\theta)$ for the arbitrary angle θ, which is a key quantity to determine H_{c2}. We can easily reconstruct $M_b(\theta)$ from the magnetization curve M_b, which is measured [38,39] because we know the experimental fact that $H_{\rm m} \propto 1/\cos\theta$. This means that the projection of M_b onto the field direction determines the magnetization curve for $M_b(\theta)$. Therefore, by projecting M_b onto the field direction, we obtain $M_b(\theta)$ for an arbitrary angle. In Fig. 4, $M_b(\theta)$ is depicted as the red curves for the relevant angles of θ. We can check this procedure for the experimental data $M_b(\theta \sim 23.7^\circ)$ for the $H \parallel (011)$ direction [39] by subtracting the contribution from the magnetization component along the c axis $M_c(\theta)$ (see also Ref. [25] for some more details).

Using these magnetization curves and the same parameter value for $\alpha_0\kappa$, we obtain $H_{\rm eff}(\theta) = H - \alpha_0\kappa M(\theta)$ as shown in Fig. 4. This indicates that for $\theta \geqslant 30^\circ$ the lower edge of $H_{\rm eff}(\theta)$ begins entering the permitted region, yielding the HSC up to $H_{c2}^{\rm AUL}$. Upon further increasing θ, $H_{\rm eff}(\theta)$ is leaving this region; thus, no HSC occurs for $\theta > 50^\circ$.

We can construct the H-T phase diagram for θ shown in Fig. 5, where the selected θ cases are depicted, including the $H \parallel b$ axis for comparison. The left-hand side bar denotes $H_{\rm eff}(\theta)$. For $\theta = 12^\circ$ the A_2 phase barely remains, beyond which there is no trace of the A_2 phase below $H_{\rm m}$ in the phase diagram. This is because $T_{c2}(M_b)$ curves (denoted in the dotted straight lines in Fig. 5), beginning at T_{c2} for $H = 0$ rotating counterclockwise owing to the decrease in the M_b projection. However, for $\theta = 35^\circ$ this T_{c2} line still reaches the metamagnetic transition field, which enables the HSC to exist above $H_{\rm m}$, as shown in Fig. 5. Thus, beginning from $H_{c2}^{\rm AUL} \sim 70$ T through $H_{\rm m}$, the H_{c2} curve extends toward $T_{c2} \sim 3$ K at $H = 0$. However, the actual HSC phase disappears abruptly at $H_{\rm m}$ because $H_{\rm eff}$ is outside the allowed region below $H_{\rm m}$. For $\theta = 45^\circ$ as only a small field region permitted for $H_{\rm eff}$ exists, as shown in the left-hand side of Fig. 5, the resulting HSC region in the H-T phase diagram shrinks. No HSC is permitted for $\theta = 50^\circ$. These features are displayed in the inset of Fig. 5.

V. DISCUSSIONS AND PERSPECTIVES

A. Parameter value of $\alpha_0\kappa$

We examine the parameter values used in this paper. The key parameter in this work is the product $\alpha_0\kappa$ of α_0 introduced in Eq. (11) and κ defined in Eq. (3). We ignore the small anisotropy of the initial slopes of H_{c2} at T_c for three field orientations of the a, b, and c axes. From the initial slopes, we find $\alpha_0 = 12$ T/1.6 K = 7.5 T/K. From the previous estimate $\kappa = 6.9\,{\rm K}/\mu_{\rm B}$ [25], which is determined by the splitting between T_{c1} and T_{c2}, and the amplitude of the ferromagnetic fluctuation moment along the a direction, we obtain $\alpha_0\kappa = 51.8\,T/\mu_{\rm B}$. From Eq. (14), we observe that

$$H_{\rm eff} = H - \alpha_0\kappa M = H - J_{\rm cf}M, \tag{18}$$

i.e., this combination is simply the form of the exchange integral $J_{\rm cf}$ between the $5f$ localized moment and conduction electrons, i.e., $J_{\rm cf} = \alpha_0\kappa$.

It is interesting to note the case in the recently found heavy Fermion superconductor $CeRh_2As_2$ [41], where $H_{c2}^c = 16$ T and $T_c = 0.35$ K. This compound is known to break the Pauli-Clogston limit $H_{\rm p} = 1.84T_c \sim 0.6$ T by far. To overcome this Pauli-Clogston limit for this spin singlet superconductor, we introduce the effective field $H_{\rm eff} = H - J_{\rm cf}M$, where the internal field is exerted from the localized 4f moment M to cancel the external applied field [36]. The exchange integral is estimated as $J_{\rm cf}^c = 52.5\,T/\mu_{\rm B}$ ($J_{\rm cf}^{ab} = 23.4/\mu_{\rm B}$) for the c axis

(*ab*-plane) in tetragonal crystal. These numbers remarkably coincide with the present system, but it may be only coincident. The important aspect is that, to achieve the high H_{c2}, we must break the Pauli-Clogston limit for a spin singlet superconductor or the orbital depairing limit for a spin triplet superconductor. Here, we propose a common mechanism in which the external field is effectively cancelled by the internal field owing to the moments of the localized f electrons through the exchange coupling to the itinerant electron system.

B. Pairing symmetry of UTe_2 and classification scheme

The present analysis clearly shows that the nonunitary state in the chiral form $d(k) = (b + ic)(k_b + ik_c)$ is suitable for UTe_2. Here, we select the orbital part $\phi(k) = k_b + ik_c$. Under applied fields, the d-vector rotates to save the Zeeman energy. This means that the spin-orbit coupling to lock the d-vector to the underlying crystal lattices is weak and finite. In other words the d-vector rotation fields $H_{\rm rot}$ depend on the field orientation, that is, $H_{\rm rot} = 5 \sim 12\,{\rm T}$ for $H \parallel b$ axis and $H_{\rm rot} = 1\,{\rm T}$ for $H \parallel c$ axis. These weak fields of $H_{\rm rot}$ indicate the strength of the spin-orbit coupling (SOC). Therefore we must adopt the weak SOC scheme for the pairing symmetry classification.

The spin-orbit coupling is anisotropic; thus, the spin space symmetry for the Cooper pairs is weakly broken from the original $SO(3)^{\rm spin}$. Furthermore, the slow ferromagnetic fluctuations also break it to split the SC transition temperature into three: T_{c1}, T_{c2}, and T_{c3}. Thus we can reasonably identify the relevant Cooper pair symmetry beginning from $SO(3)^{\rm spin}$, which is decoupled with the orbital part of the pairing function in this scheme. We emphasize that, in the strong SOC case advocated by others [42–45], the spin and orbital space symmetries are tightly coupled, the d-vector rotation cannot be permitted. As mentioned earlier, the gradual rotation of the d-vector via a second-order phase transition is accounted for only by the weak SC case. The orbital symmetry governed by the crystalline symmetry D_{2h} has no multidimensional representation. Thus the choice of the chiral form $k_b + ik_c$, which is consistent with many experiments [7–9], is ad hoc at this stage. This may indicate that the classification scheme based on the D_{2h} crystalline symmetry is irrelevant and a more larger symmetry group is required. Note that a convex curve behavior of the Sommerfeld coefficient $\gamma(H)$ at low fields for $H \parallel b$ axis associated with the Pauli paramagnetic effect [46] is an important signature of the d-vector locking and should be checked experimentally.

C. d-vector rotation

The d-vector rotation is an important concept for describing the phenomena associated with peculiar H-T phase diagrams. In particular, for $H \parallel b$ axis, the positive slope above $H \simeq 12\,{\rm T}$ can be accounted for by the d-vector rotation in which the d-vector becomes perpendicular to the b axis such that the magnetic coupling $i\mathbf{M}_b \cdot \mathbf{d} \times \mathbf{d}^*$ is active and fully utilizes magnetic energy. Otherwise, this invariant does not contribute to increasing T_{c2}. Thus the d-vector rotation is essential to capture this phenomenon.

Microscopically, the d-vector rotation occurs as a change in the spin texture formed by the spatial modulation of the three dimensional d-vector or the Cooper pair spin polarization defined by $\mathbf{S}(r) = i\mathbf{d} \times \mathbf{d}^*$. The averaged $\mathbf{S}(r)$ over the vortex unit cell determines the direction of the d-vector. The d-vector rotation is induced by the competition between the Zeeman energy and the pinning of the d-vector to the underlying lattices owing to the SOC. A microscopic theory based on quasi-classical Eilenberger equation is now in progress where intriguing spin textures, including a pair of the half-quantized vortices and Majorana zero modes both with spinless and spinful phases, are stabilized [47].

D. Chiral-nonchiral transition and β phase

When the magnetic field $H \parallel b$ axis is applied to the fully polarized nonunitary chiral p state $(a + ic)(k_b + ik_c)$, the chiral-nonchiral transition may occur. This mechanism was originally proposed by Scharnberg-Klemm [48]. This is simply because, to compare the two upper critical fields for the chiral state $(a + ic)(k_b + ik_c)$ and the nonchiral state $(a + ic)k_b$, the latter has a generally higher H_{c2}, a factor $\sim$1.5 higher for the spherical Fermi surface [49]. The line node in $(a + ic)k_b$ is robust under fields compared with $(a + ic)(k_b + ik_c)$ having the point nodes. This nonchiral state $(a + ic)k_b$ is called the β phase [1,28,29]. The β phase produced by high magnetic fields from the polar phase was recently identified in superfluid ^{3}He confined in nematic aerogel [50]. Thus it is interesting to investigate this possibility further in our superconductor. We have already identified the A_1, A_2, $A_1 + A_2$ (distorted A), and $A_1 + A_2 + A_0$ phases in lower and intermediate field regions under ambient and under pressures, respectively [23–25].

E. Application to URhGe and UCoGe

To examine the validity of the present theory, we apply it to other materials, ferromagnetic superconductors URhGe and UCoGe, which are best systems to test our concepts. Under hydrodynamic and uniaxial pressure, the H-T phase diagrams in URhGe continuously change as shown in Fig. 6. The characteristics are strikingly similar to those we have just observed, such as

(1) $T_c(H)$ increases as H increases in some part of the H-T phase diagram,

(2) the extrapolated T_c from the high field H_{c2} to high T exceeds T_{c0} at $H = 0$,

(3) the HSC is separated from LSC at low pressure,

(4) HSC and LSC overlap in high pressure region.

Let us examine these characteristics observed in URhGe in light of the present idea. It is known that under uniaxial pressure σ, the spontaneous moment M_c decreases linearly and vanishes at $\sigma = 1.2$ GPa, i.e., $M_c(\mu_{\rm B}) = 0.4 - 0.33\sigma({\rm GPa})$. It is reasonable to consider that $M_b(H) = \chi_b H$ where χ_b decreases in proportion with σ, i.e., $\chi_b = \chi_{b0} - A\sigma$ with A positive constant because the spontaneous moment M_c sets the overall magnetic scale. Thus we expect that $H_{c2}^{\rm AUL}$ is given by $H_{c2} - \alpha_0 \kappa M_c = \alpha_0 T_{c0}$, or

$$H_{c2} - \alpha_0 \kappa \chi_b H_{c2} = \alpha_0 T_{c0},$$
$$H_{c2} - \alpha_0 \kappa (\chi_{b0} - A\sigma) H_{c2} = \alpha_0 T_{c0}. \quad (19)$$

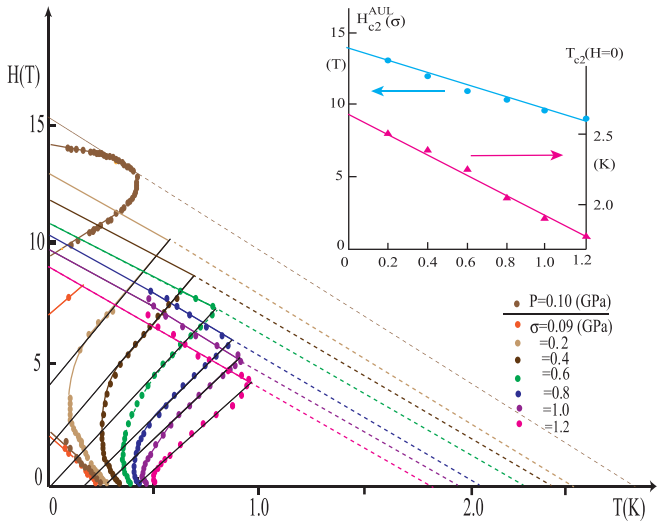

FIG. 6. H-T phase diagram under hydrodynamic (P) and uniaxial (σ) pressure for URhGe. The extrapolated straight line to lower T defines H_{c2}^{AUL} and $T_{c2}(H=0)$ to higher T, respectively. The pressure dependences of H_{c2}^{AUL} and $T_{c2}(H=0)$ are shown in the inset, indicating the linear scaling for both quantities with the linear decrease of M_c. The dotted points are the experimental data [51,52].

Equation (19) can be rewritten as

$$\frac{H_{c2}(\sigma)}{H_{c2}(\sigma=0)} = \frac{1}{1+\frac{\kappa\alpha_0 A\sigma}{1-\kappa\alpha_0\chi_0}} \simeq 1 - \frac{\kappa H_{c2}(\sigma=0) A\sigma}{T_{c0}}. \quad (20)$$

Hence $H_{c2}^{\mathrm{AUL}}(\sigma)$ decreases linearly with σ. This also implies that $T_{c2}(H=0)$ decreases linearly with σ. As shown in the inset of Fig. 6, this relation is well obeyed.

Here, we reuse our previous figure [25] on UCoGe modified slightly as Fig. 7. It is clear that H_{c2}^{AUL} also exists in UCoGe. The extrapolated $T_{c2}(H\to 0)\sim 1.0$ K is significantly higher than T_{c1}. The S-shaped H_{c2} is limited from the above, evidencing the presence of H_{c2}^{AUL}. We now understand the reason for this.

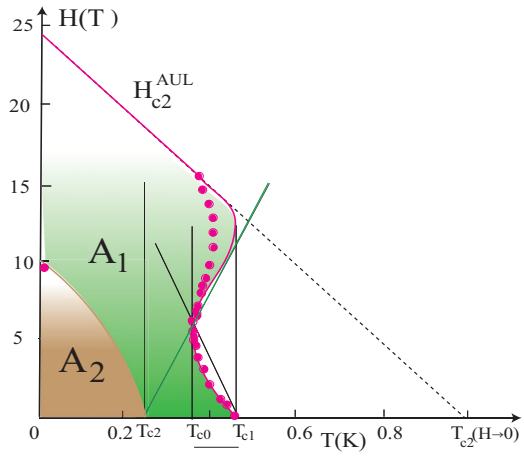

FIG. 7. H-T phase diagram [25] for $H \parallel b$ axis in UCoGe. The extrapolated straight line to lower T and higher T defines $H_{c2}^{\mathrm{AUL}} = 24$ T and $T_{c2}(H=0) = 1.0$ K, respectively. The red dots are the experimental data [53,54].

F. Perspectives

The present material UT_2 is considered to be nearly ferromagnetic, although the "static" long range ferromagnetic (FM) ordering is absent [55]. Slow FM fluctuations have been reported by several experiments [55–58]. This is similar to UPt_3, where the antiferromagnetic (AF) order above T_c is not truly static and long-ranged order, yet it leads to the spitting of T_c and significant effects on SC [23–25].

The interplay between magnetism both with FM and AF and superconductivity is an important subject and has been discussed for long time [59]. Initially, the case in which magnetism results from localized moments is considered. Thus the conduction electrons responsible for SC is distinctively different from the magnetic subsystem. This includes chevrel compounds $(RE)Rh_4B_4$ and $(RE)Mo_6S_8$ (RE: rare earth atoms). Magnetism profoundly influences SC or H_{c2} owing to the onset of AF at T_N, below which H_{c2} exhibits an anomalous kink structure associated with the destruction of a part of the Fermi surface by AF gapping [60]. For the FM, the internal FM molecular field induces Fulde-Ferrell-Larkin-Ovchinnikov state [61] immediately below the Currie temperature T_{Currie}.

These examples of the coexistence clearly differ from the present generation of the intertwining problem [62–64] in that the electrons responsible for magnetism and SC are not separable and exhibit simultaneous roles for both orderings. This duality of localized and itinerant electrons in the heavy Fermion materials is essential in forming the heavy Fermion state with the enhanced electron mass. In this case, the interplay of magnetism and SC is more intricate, which is the present scenario in UTe_2, as we have observed in this paper, the concept of the FM molecular field exerted from the magnetic sub-system is a useful one in understanding various mysteries associated with the phase diagram constructions. This continues to be valid and profitable to apply for other heavy Fermion SCs [65], including the globally or locally noncentrosymmery broken SC such as $CePt_3Si$ and $CeRh_2As_2$. These are known as the materials in which AF coexists with SC, and the anomalously enhanced H_{c2}, which breaks the Pauli-Clogston limit [36].

We admit that several outstanding issues remain to be solved in UTe_2 despite the present and previous works [23–25].

(1) Because, according to our theory, the tetra-critical point exists at $H(\parallel b)\sim 13$ T as shown in Fig. 2(a), the "fourth" second-order internal phase transition is still missing.

(2) The detailed phase diagram of HSC in $0<\theta<12^\circ$ must be investigated because it is continuously connected to the isolated HSC at $30^\circ<\theta<45^\circ$.

(3) The possible chiral-nonchiral transition for HSC should be checked experimentally. The β phase may be found.

(4) An experiment on elastic neutron scattering can probe the magnetization $M_b(H)$ component for $0^\circ<\varphi<8^\circ$ and $0^\circ<\theta<45^\circ$ to establish our reconstructed magnetization curves as shown in Figs. 3 and 4. Additionally, an experiment on small-angle neutron scattering (SANS) may reveal vortices with the spin textures for the intermediate fields of $H \parallel b$ axis.

(5) The vortex core contains the Majorana zero-energy modes spinless or spinful for HSC and LSC, respectively. These zero Majorana modes are detected through the

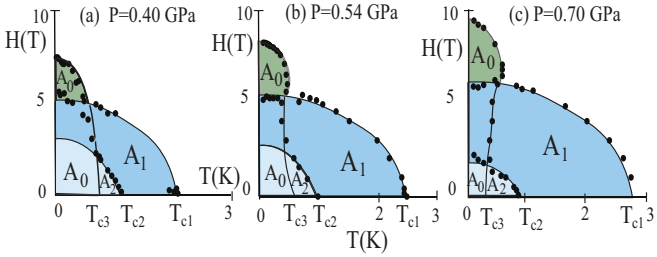

FIG. 8. H-T phase diagrams [24] for $H \parallel a$ axis where the dots are experimental data points [67] for (a) $P = 0.40$, (b) 0.54, and (c) 0.40 GPa. The labeling of various phases and transition temperatures are explained in the text of Appendix.

local density of states [66] probed using STM, or other methods.

VI. CONCLUSION AND SUMMARY

Based on a nonunitary triplet pairing state, we have found that the orbital depairing limit of H_{c2} can be exceeded by canceling the external field via the internal field exerted from the localized moments. This novel mechanism for a spin triplet state enables us to analyze the H_{c2} phase diagrams for various field orientations centered along the magnetic hard b axis. In particular, the record-high $H_{c2} \sim 70$ T occurring in between the b and the c axes can be understood by this orbital limit violation mechanism. The present work not only has identified the pairing state realized in UTe_2 but has also proposed a novel mechanism for the violation of the orbital limit of H_{c2}, which enables us to attain higher H_{c2} in a superconductor in general.

ACKNOWLEDGMENTS

The author is grateful for the enlightening discussions with D. Aoki, K. Ishida, S. Kitagawa, Y. Shimizu, S. Kittaka, T. Sakakibara, Y. Tokunaga, Y. Haga, H. Sakai, and A. Miyake. He also thanks Editage for English language editing. This work is supported by JSPS KAKENHI, No. 17K05553 and No. 21K03455

APPENDIX

To easily understand various phases appearing in the H-T phase diagrams in the main text, we summarize the naming A_1, A_2, A_0, etc. by adopting the H-T phase diagrams under pressure as a typical example. Figure 8 shows the H-T phase diagrams for (a) $P = 0.40$ GPa, (b) $P = 0.54$ GPa, and (c) $P = 0.70$ GPa for $H \parallel a$ axis [67]. As Fig. 8(a) shows, upon lowering T at T_{c1}, the A_1 phase begins to appear. Subsequently, the A_2 phase appears at T_{c2}, followed by A_0 at T_{c3}. Below T_{c2}, the two phases A_1 and A_2 are mixed to yield a mixture phase $A_1 + A_2$. Similarly below T_{c3} a mixture phase $A_1 + A_2 + A_0$ is realized. Under H, A_2 ceases to exist; thus, the mixed phase $A_1 + A_0$ continues appearing in the intermediate field region. At the highest field, only the A_0 phase remains.

As P increases from left to right in Figs. 8(a)–8(c), each phase is systematically evolving, i.e., T_{c1} increases; thus the A_1 phase enlarges. Both T_{c2} and T_{c3} decrease as P increases, leading to shrinking the areas of the A_1 and A_0 phases, but the latter survives at higher fields. The reason for it is not yet known.

For the other field orientation $H \parallel b$ axis [68], note that the transition lines beginning from T_{c2} for each P behaves similarly to those shown in Fig. 8, contrary to a naive expectation that this internal transition line joins to the tetra-critical point, i.e., there is no internal transition lines with a positive slope. This means that the fourth internal transition line occurs horizontally to the tetra-critical point, as has been observed recently [69]. This may be an important clue to understanding the phase diagram for $H \parallel b$ axis under ambient pressure [70]. For the other field orientation $H \parallel c$ axis, the experimental data [68] show relatively similar phase diagrams and systematic pressure evolution to the case for the a axis above.

[1] D. Vollhart and P. Wölfle, *The Superfluid Phases of Helium 3* (Taylor and Francis, London, 1990).

[2] T. Mizushima, Y. Tsutsumi, T. Kawakami, M. Sato, M. Ichioka, and K. Machida, Symmetry-Protected Topological Superfluids and Superconductors—From the Basics to ^{3}He—, J. Phys. Soc. Jpn. **85**, 022001 (2016).

[3] K. Machida and M. Ozaki, Superconducting Double Transition in a Heavy-Fermion Material UPt_3, Phys. Rev. Lett. **66**, 3293 (1991).

[4] T. Ohmi and K. Machida, Nonunitary Superconducting State in UPt_3, Phys. Rev. Lett. **71**, 625 (1993).

[5] Y. Machida, A. Itoh, Y. So, K. Izawa, Y. Haga, E. Yamamoto, N. Kimura, Y. Onuki, Y. Tsutsumi, and K. Machida, Twofold Spontaneous Symmetry Breaking in the Heavy-Fermion Superconductor UPt_3, Phys. Rev. Lett. **108**, 157002 (2012).

[6] Y. Tsutsumi, M. Ishikawa, T. Kawakami, T. Mizushima, M. Sato, M. Ichioka, and K. Machida, UPt_3 as a Topological Crystalline Superconductor, J. Phys. Soc. Jpn. **82**, 113707 (2013).

[7] D. Aoki, J.-P. Brison, J. Flouquet, K. Ishida, G. Knebel, Y. Tokunaga, and Y. Yanase, Unconventional Superconductivity in UTe_2, J. Phys.: Condens. Matter **34**, 243002 (2022).

[8] T. Metz, S. Bao, S. Ran, I. Lin Liu, Y. S. Eo, W. T. Fuhrman, D. F. Agterberg, S. M. Anlage, N. P. Butch, and J. Paglione, Point node gap structure of spin-triplet superconductor UTe_2, Phys. Rev. B **100**, 220504(R) (2019).

[9] S. Kittaka, Y. Shimizu, T. Sakakibara, A. Nakamura, D. Li, Y. Homma, F. Honda, D. Aoki, and K. Machida, Orientation of point nodes and nonunitary triplet pairing tuned by the easy-axis magnetization in UTe_2, Phys. Rev. Res. **2**, 032014(R) (2020).

[10] D. S. Wei, D. Saykin, O. Y. Miller, S. Ran, S. R. Saha, D. F. Agterberg, J. Schmalian, N. P. Butch, J. Paglione, and A. Kapitulnik, Interplay between magnetism and superconductivity in UTe_2, Phys. Rev. B **105**, 024521 (2022).

[11] L. Jiao, Z. Wang, S. Ran, J. O. Rodriguez, M. Sigrist, Z. Wang, N. Butch, and V. Madhavan, Microscopic evidence for a chiral

superconducting order parameter in the heavy fermion superconductor UTe_2, Nature (London) **579**, 523 (2020).

[12] G. Nakamine, S. Kitagawa, K. Ishida, Y. Tokunaga, H. Sakai, S. Kambe, A. Nakamura, Y. Shimizu, Y. Homma, D. Li, F. Honda, and D. Aoki, Superconducting properties of heavy fermion UTe_2 revealed by ^{125}Te-nuclear magnetic resonance, J. Phys. Soc. Jpn. **88**, 113703 (2019).

[13] G. Nakamine, K. Kinjo, S. Kitagawa, K. Ishida, Y. Tokunaga, H. Sakai, S. Kambe, A. Nakamura, Y. Shimizu, Y. Homma, D. Li, F. Honda, and D. Aoki, Inhomogeneous Superconducting State Probed by ^{125}Te NMR on UTe_2, J. Phys. Soc. Jpn. **90**, 064709 (2021).

[14] G. Nakamine, K. Kinjo, S. Kitagawa, K. Ishida, Y. Tokunaga, H. Sakai, S. Kambe, A. Nakamura, Y. Shimizu, Y. Homma, D. Li, F. Honda, and D. Aoki, Anisotropic response of spin susceptibility in the superconducting state of UTe_2 probed with ^{125}Te-NMR measurement, Phys. Rev. B **103**, L100503 (2021).

[15] H. Fujibayashi, G. Nakamine, K. Kinjo, S. Kitagawa, K. Ishida1, Y. Tokunaga, H. Sakai, S. Kambe, A. Nakamura, Y. Shimizu, Y. Homma, D. Li, F. Honda, and D. Aoki, Superconducting Order Parameter in UTe_2 Determined by Knight Shift Measurement, J. Phys. Soc. Jpn. **91**, 043705 (2022).

[16] K. Kinjo, H. Fujibayashi, S. Kitagawa, K. Ishida, Y. Tokunaga, H. Sakai, S. Kambe, A. Nakamura, Y. Shimizu, Y. Homma, D. X. Li, F. Honda, D. Aoki, K. Hiraki, M. Kimata, and T. Sasaki, Magnetic field-induced transition with spin rotation in the superconducting phase of UTe_2, Phys. Rev. B **107**, L060502 (2023)>.

[17] It should be noted that in a dirty superconductor, H_{c2} can be arbitrarily large in principle because the effective coherent length is given by a symbolic formula $1/\xi_{\rm eff} \propto 1/l + 1/\xi$ with l being the transport mean free path.

[18] D. Aoki, H. Sakai, P. Opletal, Y. Tokiwa, J. Ishizuka, Y. Yanase, H. Harima, A. Nakamura, D. Li, Y. Homma, Y. Shimizu, G. Knebel, J. Flouquet, and Y. Haga, First observation of the de haas-van alphen effect and fermi surfaces in the unconventional superconductor UTe_2, J. Phys. Soc. Jpn. **91**, 083704 (2022).

[19] A. Rosuel, C. Marcenat, G. Knebel, T. Klein, A. Pourret, N. Marquardt, Q. Niu, S. Rousseau, A. Demuer, G. Seyfarth, G. Lapertot, D. Aoki, D. Braithwaite, J. Flouquet, and J. P. Brison, Field-Induced Tuning of the Pairing State in a Superconductor, Phys. Rev. X **13**, 011022 (2023).

[20] T. Helm, M. Kimata, K. Sudo, A. Miyata, J. Stirnat, T. Förster, J. Hornung, M. König, I. Sheikin, A. Pourret, G. Lapertot, D. Aoki, G. Knebel, J. Wosnitza, and J.-P. Brison, Field-induced compensation of magnetic exchange as the origin of superconductivity above 40 T in UTe_2, arXiv:2207.08261.

[21] G. Knebel, W. Knafo, A. Pourret, Q. Niu, M. Vališka, D. Braithwaite, G. Lapertot, M. Nardone, A. Zitouni, S. Mishra, I. Sheikin, G. Seyfarth, J.-P. Brison, D. Aoki, and J. Flouquet, Field-reentrant superconductivity close to a metamagnetic transition in the heavy-fermion superconductor UTe_2, J. Phys. Soc. Jpn. **88**, 063707 (2019).

[22] A. Ramires, Nonunitary superconductivity in complex quantum materials, J. Phys.: Condens. Matter **34**, 304001 (2022).

[23] K. Machida, Theory of spin-polarized superconductors–an analogue of superfluid ^{3}He A-phase–, J. Phys. Soc. Jpn. **89**, 033702 (2020).

[24] K. Machida, Notes on multiple superconducting phases in UTe_2–Third Transition–, J. Phys. Soc. Jpn. **89**, 065001 (2020).

[25] K. Machida, Nonunitary triplet superconductivity tuned by field-controlled magnetization: URhGe, UCoGe, and UTe_2, Phys. Rev. B **104**, 014514 (2021).

[26] K. Machida and T. Ohmi, Phenomenological Theory of Ferromagnetic Superconductivity, Phys. Rev. Lett. **86**, 850 (2001).

[27] J. F. Annett, Symmetry of the order parameter for high-temperature superconductivity, Adv. Phys. **39**, 83 (1990).

[28] Masa-aki Ozaki, K. Machida, and T. Ohmi, On p-Wave Pairing Superconductivity under Cubic Symmetry, Prog. Theor. Phys. **74**, 221 (1985).

[29] Masa-aki Ozaki, K. Machida, and T. Ohmi, On p-wave pairing superconductivity under hexagonal and tetragonal symmetries, Prog. Theor. Phys. **75**, 442 (1986).

[30] V. Ambegaokar and N. D. Mermin, Thermal Anomalies of He^3: Pairing in a Magnetic Field, Phys. Rev. Lett. **30**, 81 (1973).

[31] K. Machida, T. Ohmi, and M. Ozaki, Anisotropy of upper critical fields for d- and p-wave pairing superconductivity, J. Phys. Soc. Jpn. **54**, 1552 (1985).

[32] K. Machida, M. Ozaki, and T. Ohmi, Unconventional superconducting class in a heavy fermion system UPt_3, J. Phys. Soc. Jpn. **59**, 4223 (1990).

[33] K. Machida, T. Fujita, and T. Ohmi, Vortex Structures in an Anisotropic Pairing Superconducting State with Odd-Parity, J. Phys. Soc. Jpn. **62**, 680 (1993).

[34] K. Machida, T. Nishira, and T. Ohmi, Orbital symmetry of a triplet pairing in a heavy fermion superconductor UPt_3, J. Phys. Soc. Jpn. **68**, 3364 (1999).

[35] M. Tinkham, *Introduction to Superconductivity* (McGraw-Hill, New York, 1975).

[36] K. Machida, Violation of Pauli-Clogston limit in the heavy-fermion superconductor $CeRh_2As_2$: Duality of itinerant and localized 4f electrons, Phys. Rev. B **106**, 184509 (2022).

[37] V. Jaccarino and M. Peter, Ultra-High-Field Superconductivity, Phys. Rev. Lett. **9**, 290 (1962).

[38] A. Miyake, Y. Shimizu, Y. J. Sato, D. Li, A. Nakamura, Y. Homma, F. Honda, J. Flouquet, M. Tokunaga, and D. Aoki, Metamagneitc transition in heavy Fermion superconductor UTe_2, J. Phys. Soc. Jpn. **88**, 063706 (2019).

[39] A. Miyake, Y. Shimizu, Y. J. Sato, D. Li, A. Nakamura, Y. Homma, F. Honda, J. Flouquet, M. Tokunaga, and D. Aoki, Enhancement and discontinuity of effective mass through the first-order metamagnetic transition in UTe_2, J. Phys. Soc. Jpn. **90**, 103702 (2021).

[40] S. Nakamura, T. Sakakibara, Y. Shimizu, S. Kittaka, Y. Kono, Y. Haga, J. Pospíšil, and E. Yamamoto, Wing structure in the phase diagram of the Ising ferromagnet URhGe close to its tricritical point investigated by angle-resolved magnetization measurements, Phys. Rev. B **96**, 094411 (2017).

[41] S. Khim, J. F. Landaeta, J. Banda, N. Bannor, M. Brando, P. M. R. Brydon, D. Hafner, R. Küchler, R. Cardoso-Gil, U. Stockert, A. P. Mackenzie, D. F. Agterberg, C. Geibel, and E. Hassinger, Field-induced transition within the superconducting state of $CeRh_2As_2$, Science **373**, 1012 (2021).

[42] P. W. Anderson, Structure of "triplet" superconducting energy gaps, Phys. Rev. B **30**, 4000 (1984).

[43] E. I. Blount, Symmetry properties of triplet superconductors, Phys. Rev. B **32**, 2935 (1985).

[44] G. E. Volovik and L. P. Gor'kov, Superconducting classes in heavy-fermion systems, Sov. Phys. JETP **61**, 843 (1985).

[45] R. Joynt and L. Taillefer, The superconducting phases of UPt_3, Rev. Mod. Phys. **74**, 235 (2002).

[46] K. Machida and M. Ichioka, Magnetic field dependence of low-temperature specific heat in Sr_2RuO_4, Phys. Rev. B **77**, 184515 (2008).

[47] Y. Tsutsumi and K. Machida (unpublished).

[48] K. Scharnberg and R. A. Klemm, Upper Critical Field in *p*-Wave Superconductors with Broken Symmetry, Phys. Rev. Lett. **54**, 2445 (1985).

[49] P. Miranović, N. Nakai, M. Ichioka, and K. Machida, Orientational field dependence of low-lying excitations in the mixed state of unconventional superconductors, Phys. Rev. B **68**, 052501 (2003).

[50] V. V. Dmitriev, M. S. Kutuzov, A. A. Soldatov, and A. N. Yudin, Superfluid β Phase in Liquid ^{3}He, Phys. Rev. Lett. **127**, 265301 (2021).

[51] A. Miyake, D. Aoki, and J. Flouquet, Pressure evolution of the ferromagnetic and field re-entrant superconductivity in URhGe, J. Phys. Soc. Jpn. **78**, 063703 (2009).

[52] D. Braithwaite, D. Aoki, J.-P. Brison, J. Flouquet, G. Knebel, A. Nakamura, and A. Pourret, Dimensionality Driven Enhancement of Ferromagnetic Superconductivity in URhGe, Phys. Rev. Lett. **120**, 037001 (2018).

[53] D. Aoki, T. D. Matsuda, V. Taufour, E. Hassinger, G. Knebel, and J. Flouquet, Extremely large and anisotropic upper critical field and the ferromagnetic instability in UCoGe, J. Phys. Soc. Jpn. **78**, 113709 (2009).

[54] B. Wu, G. Bastien, M. Taupin, C. Paulsen, L. Howard, D. Aoki, and J.-P. Brison, Pairing mechanism in the ferromagnetic superconductor UCoGe, Nat. Commun. **8**, 14480 (2017).

[55] S. Sundar, S. Gheidi, K. Akintola, A. M. Côté, S. R. Dunsiger, S. Ran, N. P. Butch, S. R. Saha, J. Paglione, and J. E. Sonier, Coexistence of ferromagnetic fluctuations and superconductivity in the actinide superconductor UTe_2, Phys. Rev. B **100**, 140502(R) (2019).

[56] Y. Tokunaga, H. Sakai, S. Kambe, T. Hattori, N. Higa, G. Nakamine, S. Kitagawa, K. Ishida, A. Nakamura, Y. Shimizu, Y. Homma, DeXin Li, F. Honda, and D. Aoki, ^{125}Te-NMR study on a single crystal of heavy fermion superconductor UTe_2, J. Phys. Soc. Jpn. **88**, 073701 (2019).

[57] Y. Tokunaga, H. Sakai, S. Kambe, Y. Haga, Y. Tokiwa, P. Opletal, H. Fujibayashi, K. Kinjo, S. Kitagawa, K. Ishida, A. Nakamura, Y. Shimizu, Y. Homma, D. Li, F. Honda, and D. Aoki, Slow electronic dynamics in the paramagnetic state of UTe_2, J. Phys. Soc. Jpn. **91**, 023707 (2022).

[58] D. V. Ambika, Q.-P. Ding, K. Rana, C. E. Frank, E. L. Green, S. Ran, N. P. Butch, and Y. Furukawa, Possible coexistence of antiferromagnetic and ferromagnetic spin fluctuations in the spin-triplet superconductor UTe_2 revealed by ^{125}Te NMR under pressure, Phys. Rev. B **105**, L220403 (2022).

[59] K. Machida, Spin density wave and superconductivity in highly anisotropic materials, J. Phys. Soc. Jpn. **50**, 2195 (1981); K. Machida and T. Matsubara, Spin density wave and superconductivity in highly anisotropic materials. II. Detailed study of phase transitions, **50**, 3231 (1981).

[60] K. Machida, K. Nokura, and T. Matsubara, Theory of antiferromagnetic superconductors, Phys. Rev. B **22**, 2307 (1980).

[61] K. Machida and H. Nakanishi, Superconductivity under a ferromagnetic molecular field, Phys. Rev. B **30**, 122 (1984).

[62] K. Machida and M. Kato, Inherent Spin-Density-Wave Instability in Heavy-Fermion Superconductivity, Phys. Rev. Lett. **58**, 1986 (1987).

[63] E. Fradkin, S. A. Kivelson, and J. M. Tranquada, Theory of intertwined orders in high temperature superconductors, Rev. Mod. Phys. **87**, 457 (2015).

[64] B. Keimer, S. A. Kivelson, M. R. Norman, S. Uchida, and J. Zaanen, From quantum matter to high-temperature superconductivity in copper oxides, Nature (London) **518**, 179 (2015).

[65] C. Pfleiderer, Superconducting phase of f-electron compounds, Rev. Mod. Phys. **81**, 1551 (2009).

[66] M. Ichioka, N. Hayashi, and K. Machida, Local density of states in the vortex lattice in a type-II superconductor, Phys. Rev. B **55**, 6565 (1997).

[67] D. Aoki, F. Honda, G. Knebel, D. Braithwaite, A. Nakamura, DeXin Li, Y. Homma, Y. Shimizu, Y. J. Sato, J.-P. Brison, and J. Flouquet, Multiple superconducting phases and unusual enhancement of the upper critical field in UTe_2, J. Phys. Soc. Jpn. **89**, 053705 (2020).

[68] D. Aoki *et al.* (unpublished).

[69] H. Sakai, Y. Tokiwa, P. Opletal, M. Kimata, S. Awaji, T. Sasaki, D. Aoki, S. Kambe, Y. Tokunaga, and Y. Haga, Field Induced Multiple Superconducting Phases in UTe_2 along Hard Magnetic Axis, Phys. Rev. Lett. **130**, 196002 (2023).

[70] K. Machida (unpublished).